

High-Efficiency Photovoltaic Conversion at Selective Electron Tunneling Heterointerfaces

Chuan Cheng Jia, Wei Ma, Jianxin Guan, Chunhui Gu, Xinxi Li, Linan Meng, Yao Gong, Sheng Meng,* and Xuefeng Guo*

Effectively controlling photoinduced charge transport at the heterointerface is of crucial importance for improving the performance of photovoltaic devices. On the basis of an ipsilateral selective electron tunneling (ISET) mechanism, here this study investigates photoinduced charge transport and photovoltaic conversion at a simplified dye/single-layer graphene (SLG)/TiO₂ ternary interface. With an amphiphilic Z907 molecule as the model dye, the photoexcited electrons in the dye can directly tunnel across SLG and be collected by the TiO₂ layer with an efficiency of 96.23%, which guarantees a high-efficiency photoelectric conversion at the ISET-based heterointerface. More importantly, the intrinsic Schottky barrier and fast hole collection rate at the heterointerface lead to a high photovoltage, a large fill factor, and the good intense-light performance for photovoltaic conversion. Such an ISET-based heterointerface may offer a platform of designing and developing a novel class of photovoltaic devices with high efficiency.

1. Introduction

Photoinduced charge transport in heterostructures is the core of most detectors,^[1,2] sensors,^[3,4] photoswitches,^[5–7] and photovoltaic devices.^[8–11] By effectively controlling charge transport at the heterointerface, specific functions can be realized, and the operating efficiencies can be improved in these devices. In

particular, highly efficient photogenerated electron–hole pair separation, transport, and collection at the heterointerface are the key to achieve high photon-to-current conversion efficiency for photovoltaic devices.^[12–15] Therefore, interface engineering was widely applied to control the photoinduced charge transport processes at the heterointerface for improving the performance of photovoltaic devices.^[16–19]

Recently, we discovered an ipsilateral selective electron tunneling (ISET) mechanism, which can be used to effectively separate photoinduced electron–hole pair at the heterointerface.^[20,21] Specifically, when photoactive materials are assembled on the outside surface of single-layer graphene (SLG)/TiO₂, Schottky diode, photoexcited electrons, as well as holes

produced from the photoactive materials transport along the same direction to SLG, whereas only electron can further inject into the TiO₂ layer, thus realizing photogenerated electron–hole pair separation at the Schottky interface. With acridine orange (AO) dye as a model photoactive material, ≈86.8% photocarrier separation/collection efficiency was realized at the AO/SLG/TiO₂ interface. Therefore, such an ISET effect at the heterointerface has great potential to be applied for efficient photovoltaic conversion.

Due to a highly photoactive and unique amphiphilic structure, Z907 ruthenium molecules were widely used as the dye sensitizer in all-solid-state dye-sensitized solar cells.^[22] In this work, Z907 molecules were chosen as the photoactive material to construct a Z907/SLG/TiO₂ ternary interface. As shown in **Figure 1a**, the photoexcited electrons in Z907 molecules are expected to tunnel across SLG and ballistically inject into the conduction band (CB) of the TiO₂ semiconductor layer, while photoexcited holes in Z907 molecules can only transport to the SLG semimetal layer. After that, the electron and hole are collected by the TiO₂ layer and the SLG layer, respectively, and further transport to the outside circuit for photoelectric conversion. Based on such an ISET mechanism, the electron transparency of the graphene layer is crucial for the high-efficiency photovoltaic conversion in ISET-based photovoltaic devices. Considering the fact that the electron transparency decreases with increasing the thickness of graphene,^[23] single-layer graphene was chosen to construct the ISET-based heterointerface. With such an ISET-based heterointerface, we investigated the photoinduced carrier dynamic processes and photoelectric conversion performances at the heterointerface.

Dr. C. Jia, J. Guan, C. Gu, X. Li, Y. Gong, Prof. X. Guo
 Beijing National Laboratory for Molecular Sciences
 State Key Laboratory for Structural Chemistry
 of Unstable and Stable Species
 College of Chemistry and Molecular Engineering
 Peking University
 Beijing 100871, China
 E-mail: guoxf@pku.edu.cn

Dr. W. Ma, L. Meng, Prof. S. Meng
 Beijing National Laboratory for Condensed Matter Physics
 Institute of Physics
 Chinese Academy of Sciences
 Beijing 100190, China
 E-mail: smeng@iphy.ac.cn

Dr. W. Ma, L. Meng, Prof. S. Meng
 Collaborative Innovation Center of Quantum Matter
 Beijing 100190, China
 Prof. X. Guo
 Department of Materials Science and Engineering
 College of Engineering
 Peking University
 Beijing 100871, China

 The ORCID identification number(s) for the author(s) of this article can be found under <https://doi.org/10.1002/aelm.201700211>.

DOI: 10.1002/aelm.201700211

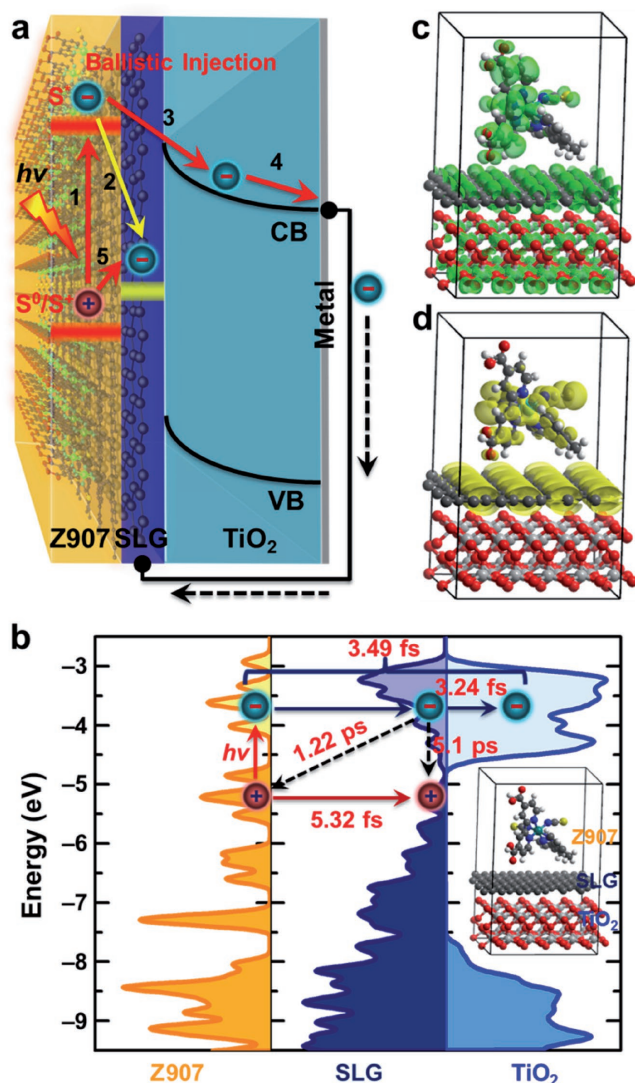


Figure 1. ISET mechanism at the Z907/SLG/TiO₂ ternary interface. a) Schematic of the processes of photoinduced carrier generation, separation, and transport in photovoltaic devices with a Z907/SLG/TiO₂ ternary interface. b) PDOS spectra for Z907, SLG, and TiO₂, showing the electronic structures of the heterointerface. Left inset shows the structure of the simulated heterointerface containing a rutile TiO₂ (001) layer, an SLG layer, and a simplified Z907 molecule with optimized configuration. c) Charge densities at -3.7 eV, where the delocalized distribution on the whole Z907/SLG/TiO₂ leads to direct electron tunneling from Z907 to the TiO₂ layer. d) Charge densities at -5.2 eV, where the localized distribution on Z907 and the SLG layer gives rise to hole transfer from Z907 to SLG.

2. Results and Discussion

To explore the ISET mechanism at the heterointerface, a model Z907/SLG/TiO₂ system (inset of Figure 1b) was calculated by the first-principles density functional theory.^[24] From the calculated projected density-of-states (PDOS) spectra (Figure 1b), it can be observed that the lowest unoccupied molecular orbit (LUMO) of Z907 molecules, located at about -3.7 eV versus the vacuum level, is well matched to the unoccupied electronic states of the SLG layer, which is tightly coupled to the CB states of the TiO₂ layer. Furthermore, the charge density distribution

at -3.7 eV (Figure 1c) is also found delocalized on the whole Z907/SLG/TiO₂ system. With such matched electronic states, the photoinduced electrons could directly tunnel from LUMO of Z907 molecules to CB of the TiO₂ layer, which is similar to the case of charge transport in single-molecule devices.^[25–27] On the other hand, the highest occupied molecular orbit (HOMO) of Z907 molecules, lying at ≈ -5.2 eV, just matches the occupied states of SLG, where there is no matched energy band in the TiO₂ layer. For charge densities at -5.2 eV (Figure 1d), they just distribute in the Z907 and SLG layers. Therefore, the photoinduced holes could just transfer from HOMO of Z907 molecules to the SLG layer, thus realizing the ipsilateral photoinduced hole–electron pair separation at the heterointerface.

Furthermore, the dynamic processes of such an ISET-based carrier transfer at the Z907/SLG/TiO₂ ternary interface were theoretically studied by the fewest-switching-surface-hopping method.^[28,29] Based on theoretical simulations, the electrons on LUMO of Z907 can directly inject from Z907 to CB of the TiO₂ layer across the SLG layer with a lifetime of $\tau_{e\text{-TiO}_2} \approx 3.49$ fs (Figure S1a and Table S1, Supporting Information).^[30] In contrast, the holes on HOMO of Z907 can just inject from Z907 to the SLG layer with a lifetime of $\tau_{h\text{-SLG}} \approx 5.32$ fs (Figure S1b, Supporting Information).^[31] In addition, the passing electrons on SLG could possibly inject into TiO₂ with a lifetime of $\tau_{\text{SLG-TiO}_2} \approx 3.24$ fs (Figure S2, Supporting Information),^[32] and recombine with the hole on the Z907 molecule at a time scale of $\tau_{\text{rec-Z907}} \approx 1.22$ ps (Figure S3, Supporting Information).^[33] Considering the intrinsic hot electron relaxation on graphene ($\tau_{\text{rel}} \approx 5.1$ ps),^[20] the efficiency for electron tunneling across the SLG layer can be calculated by the formula $(1/\tau_{\text{SLG-TiO}_2})/(1/\tau_{\text{rec-Z907}} + 1/\tau_{\text{rel}} + 1/\tau_{\text{SLG-TiO}_2})$, which affords a value of 99.7%. This value is a harbinger for the high-efficiency photogenerated carrier separation at the heterointerface described below.

To experimentally explore the charge transfer dynamics and photovoltaic conversion processes at such an ISET-based heterointerface, a model Z907/SLG/TiO₂ ternary interface and the corresponding photovoltaic device were fabricated. A schematic of the overall structure of the photovoltaic device was shown in Figure 2a. The detailed fabrication process was given in the Supporting Information. In brief, rutile TiO₂ (001) single crystals with an atomically flat surface, confirmed by atomic force microscopy (AFM) characterization (Figure S4a, Supporting Information), was used as the semiconductor layer. Graphene was obtained by a low-pressure chemical vapor deposition (CVD) process under optimal conditions^[34] and was further transferred onto the TiO₂ surface by using an isopropanol-assisted dry-transfer method with a poly(methyl methacrylate) (PMMA) support layer.^[35] The Raman spectrum of the grown graphene was shown in Figure 2c (black line), where a single narrow symmetric 2D peak (≈ 2660 cm⁻¹), small G/2D ratio, and negligible D peak indicate that SLG with high quality was used.^[36,37] The Z907 dye was dispersed on the SLG surface under an optimized spin-coating condition of 1500 rpm and further annealed for realizing ascendant configuration on the SLG surface. AFM characteristics in Figure 2b demonstrate that a compact Z907 monolayer with ≈ 1.6 nm thickness was prepared. From the Raman spectrum (red line in Figure 2c), it can be observed that characteristic peaks of Z907 molecules appear,

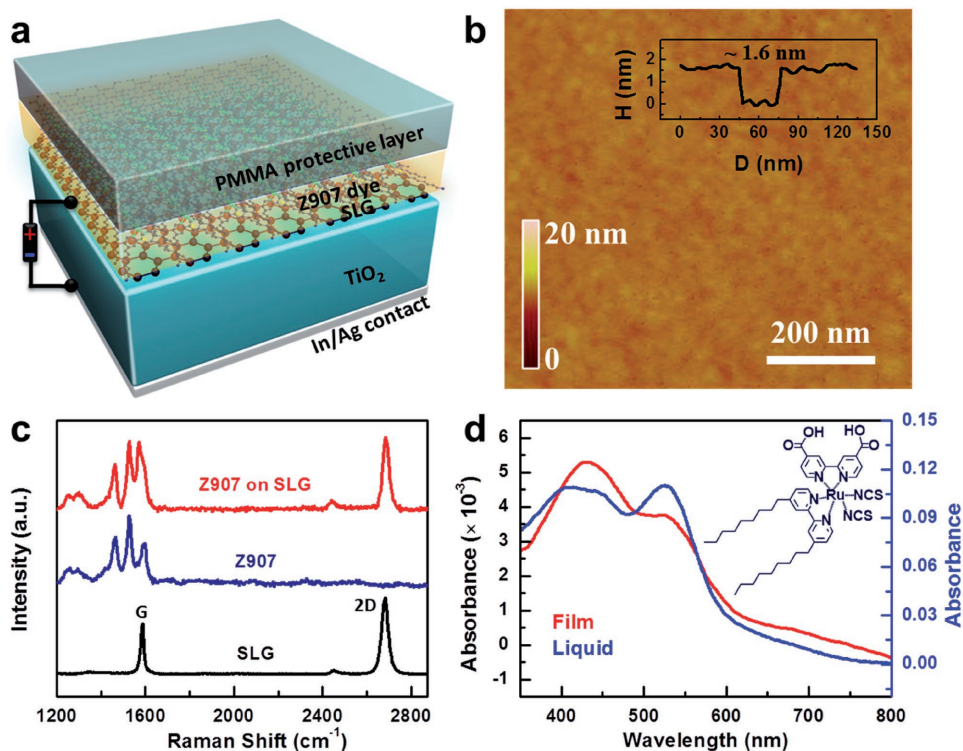


Figure 2. Device structure and characteristics. a) Schematic of a designed photovoltaic device with the Z907/SLG/TiO₂ ternary interface. b) AFM image of the Z907/SLG/TiO₂ surface, indicating the formation of a uniform high-coverage Z907 monolayer with 1.6 ± 0.1 nm thickness. c) Raman spectra of a CVD-grown SLG (black), a pure Z907 dye (blue), and a Z907 monolayer assembled on SLGs (red). d) UV-vis absorption spectra of Z907 in solution (blue line) and assembled on SLG (red line). The inset shows the chemical structure of Z907 molecules.

which range from 1400 to 1600 cm⁻¹ and belong to the framework vibration of the aromatic rings,^[38] indicating that Z907 molecules were successfully assembled on the SLG surface. The success of the Z907 assembly on SLGs was also confirmed by X-ray photoelectron spectroscopic characteristics (Figure S5, Supporting Information). In addition, the UV-vis absorption spectrum for the Z907 monolayer assembled on SLGs (red line in Figure 2d) shows two characteristic peaks at ≈420 nm and ≈510 nm. In comparison with the absorption spectrum of Z907 in solution (blue line in Figure 2d), there is some reduction at the 510 nm absorption peak for Z907 on SLGs, which is consistent with the theoretical simulated UV-vis absorption of Z907 molecules (Figure S6, Supporting Information). On the top of the Z907 monolayer, there was a PMMA protective layer, which was fabricated by a spin-coating method. For fabricating photovoltaic devices, 100 nm In and 100 nm Ag, which were thermally evaporated on the back side of TiO₂, were used as Ohmic contact electrodes.

The competing kinetic processes between photogenerated carrier separation/collection and recombination at the ternary interface determine the performance of photovoltaic devices.^[12,39] In order to explore these competing processes, the charge transfer dynamic processes at the Z907/SLG/TiO₂ ternary interface was first investigated by a transient photoluminescence (PL) method.^[40] With Z907 dyes dispersed in a PMMA matrix, the intrinsic PL decay processes of Z907 dye was measured. From the PL decay spectrum (black in Figure 3a), the intrinsic interband recombination lifetime

of Z907 excitons was obtained with a value of $\tau_1 = 39.24$ ns, which corresponds to the dominant PL decay time calculated by data fitting (Table S2, Supporting Information). When the Z907 dye was assembled on a suspending SLG, a dominant PL decay with a lifetime of $\tau_2 = 8.37$ ns occurred (blue in Figure 3a), which is related to the photoexcited electron transfer from Z907 to SLG. For Z907/SLG further attached on the TiO₂ surface, the dominant PL decay was decreased to $\tau_3 = 0.27$ ns, which is attributed to the excited electron tunneling transfer from Z907 to TiO₂. The photogenerated electron collection efficiency at the heterointerface can be calculated with the formula $(1/\tau_3)/(1/\tau_1 + 1/\tau_2 + 1/\tau_3)$, which affords a value of ≈96.23%, a guarantee of high photoelectric conversion efficiency for Z907/SLG/TiO₂-based photovoltaic devices.

As the interfacial hole transfer is the rate-limiting process for most photovoltaic devices,^[41] the transient photovoltage method was used to explore such rate-limiting hole transfer processes in ISET-based photovoltaic devices.^[20,42] With photoexcitation by a 532 nm pulse laser, the transient photovoltage spectrum of the Z907/SLG/TiO₂ photovoltaic device was monitored by an oscilloscope.^[43] As shown in Figure 3b, the transient photovoltage rise times of the devices are well fitted to a double-exponential curve as follows: $V = 24.09 - 14.93 \times \exp(-t/113.81) - 14.15 \times \exp(-t/339.69)$ with a mean square error of 0.9513, where V is the transient photovoltage value in unit of millivolt (mV) and t is the evolution time in unit of microsecond (μ s). The fast rise time constant ($\tau_e = 113.81 \mu$ s) is attributed to the process of photoelectron injection into the TiO₂ layer and further transfer

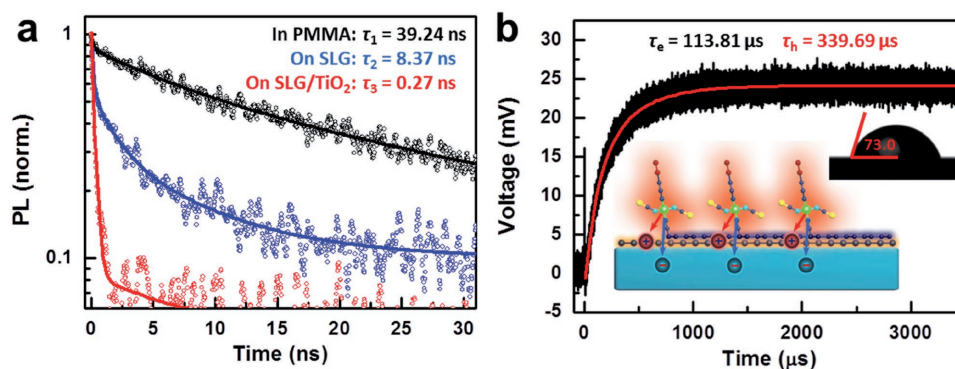


Figure 3. Interfacial charge separation/transport dynamics. a) Normalized time-resolved PL spectrum for the Z907 dye dispersed in a PMMA matrix (black), assembled on SLG (blue), and assembled on an SLG/TiO₂ interface (red). The dominant PL decay time (τ) constants are summarized in Table S2 (Supporting Information). b) Transient photovoltage measurements of the Z907/SLG/TiO₂ device, where the data were fitted to a double exponential curve (red line). The left inset shows the result of contact angle measurements, which indicates the hydrophilic character of the Z907/SLG/TiO₂ surface. The right inset shows the schematic of the photogenerated carrier transfer processes at the Z907/SLG/TiO₂ interface, where the alkyl chains of Z907 molecules are attached to the SLG surface.

to the In/Ag back electrode. As electron transfer in the uniform TiO₂ layer is a rate-limiting step, the time constant τ_e is similar to that in the control SLG/Z907/TiO₂ photovoltaic device with a value of $\approx 101.97 \mu\text{s}$ (Figure S8a, Supporting Information). In contrast, the slow rise time constant ($\tau_h = 339.69 \mu\text{s}$) corresponds to hole transfer from HOMO of excited Z907 molecules to the SLG layer, which is shorter than that of $\approx 739.77 \mu\text{s}$ for the control device. From both contact angle measurement (inset of Figure 3b) and theoretical simulation (Figure S9, Supporting Information), it can be confirmed that the alkyl chain groups in Z907 molecules are attached to the surface of graphene, leading the photoactive Ru coordination close to the SLG layer. In addition, as the photogenerated electron and hole transport to the same direction at the Z907/SLG/TiO₂ interface and the opposite direction in the control SLG/Z907/TiO₂ interface, the electrostatic attraction between electron and hole is expected to accelerate the hole transport process in the Z907/SLG/TiO₂ system and slow the hole transport process in the control system (Figure S10, Supporting Information). Therefore, with such a preponderant conformation of Z907 assembly and the electrostatic attraction effect between electron-hole pairs, the photogenerated holes transfer to the SLG layer at a faster speed at the ISET-based heterointerface.

Based on the superior charge separation/transport dynamics at the Z907/SLG/TiO₂ ternary interface, a model photovoltaic device was developed for studying the photovoltaic conversion at the heterointerface. Current-voltage characteristics of a working device and a control device without the Z907 dye were measured in the dark and under visible light ($>420 \text{ nm}$, 90 mW cm^{-2}) illumination. As shown in Figure 4a, both the working device and the control device in the dark exhibited similar rectifying characteristics, indicating that a Schottky barrier was well formed at the SLG/TiO₂ interface and the assembled Z907 dye had negligible effect on the Schottky barrier. Under illumination, the working device exhibited an open-circuit voltage (V_{OC}) of $\approx 0.663 \text{ V}$, a short-circuit current density (J_{SC}) of $\approx 3.27 \mu\text{A cm}^{-2}$, and a fill factor (FF) of ≈ 0.5199 (Table S3, Supporting Information). However, the control device without Z907 showed the negligible photocurrent

response, proving that the photoresponse of the Z907/SLG/TiO₂ device mainly originates from the photoexcited Z907 dye, rather than either the photoexcitation of the SLG layer^[44] or the TiO₂ layer. In addition, a parallel control SLG/Z907/TiO₂ device with traditional photovoltaic mechanism was also investigated at the same conditions, which had a photovoltaic conversion performance of $V_{\text{OC}} \approx 0.580 \text{ V}$, $J_{\text{SC}} \approx 4.91 \mu\text{A cm}^{-2}$, and $\text{FF} \approx 0.3467$ (Figure S11 and Table S4, Supporting Information). Consequently, the V_{OC} and FF values of the Z907/SLG/TiO₂ device are larger than those of the control SLG/Z907/TiO₂ device, which illustrates the more effective photovoltaic conversion at the ISET-based heterointerface.

For further studying the photovoltaic conversion at the Z907/SLG/TiO₂ heterointerface, light-intensity-dependent photovoltaic performances of the model device were measured (Figure S12, Supporting Information). With the light intensity increased from 2.26 to 90 mW cm^{-2} , the J_{SC} values linearly increased from 0.092 to $3.27 \mu\text{A cm}^{-2}$ (Figure 4b). At the same time, with increasing the light intensity, the V_{OC} values gradually increased from 0.469 to 0.633 eV (Figure 4c), which indicates that V_{OC} of the devices is determined by both the intrinsic Schottky barrier at the SLG/TiO₂ interface and the photoexcitation of the Z907 dye. For the control SLG/Z907/TiO₂ device, with the same light intensities, V_{OC} increased from 0.415 to 0.580 eV (Figure S14a, Supporting Information), which is smaller than that of the Z907/SLG/TiO₂ device at all light intensities. For the fill factor of the Z907/SLG/TiO₂ device, with increasing the light intensity, it slightly decreased from 0.572 to 0.520 (Figure 4d), while for the control SLG/Z907/TiO₂ device, it markedly decreased from 0.540 to 0.347 (Figure S14c, Supporting Information). As the fill factor of the photovoltaic device reflects the inherent photocarrier recombination during the photovoltaic processes,^[45,46] there is little recombination for the ISET-based photovoltaic conversion at the Z907/SLG/TiO₂ ternary interface, even under intense light radiation. Correspondingly, the overall photon-to-electron conversion efficiency (η) peak value appears at $\approx 30 \text{ mW cm}^{-2}$ for the Z907/SLG/TiO₂ device, which was much larger than that of the SLG/Z907/TiO₂ control device with a value of $\approx 10 \text{ mW cm}^{-2}$, further confirming

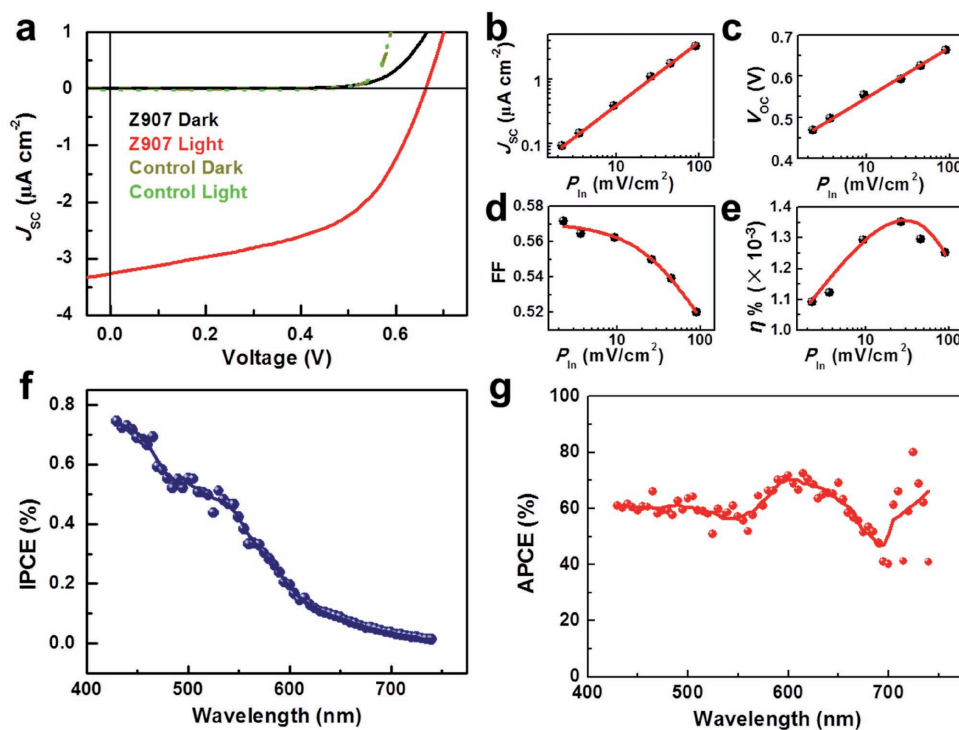


Figure 4. Photovoltaic characteristics. a) Current–voltage characteristics of the Z907/SLG/TiO₂ photovoltaic device measured in the dark (black line) and under visible light (>420 nm, 90 mW cm⁻²) illumination (red line). For comparison, a control device without the Z907 dye was also studied in the dark (dark yellow line) and under the same visible light illumination (green line). b–e) Light-intensity-dependent b) V_{OC}, c) J_{SC}, d) FF, and e) η of the Z907/SLG/TiO₂ device. f) The IPCE spectrum of the photovoltaic device. g) The APCE spectrum of the device that demonstrates an internal quantum efficiency of ≈60%.

that the Z907/SLG/TiO₂ heterointerface could effectively separate the photocarriers generated under intense light radiation.

To evaluate the photoelectric conversion efficiency at the Z907/SLG/TiO₂ heterointerface, the incident photon-to-current conversion efficiency (IPCE) for the Z907/SLG/TiO₂ device was measured as a function of photoexcitation wavelength. The light harvesting efficiency (LHE) of the assembled Z907 monolayer was converted from its absorption spectrum shown in red line of Figure 2d. As the IPCE spectrum of the device (Figure 4f) and the LHE spectrum of the Z907 monolayer (Figure S15, Supporting Information) share the similar shape characteristics in the 420–740 nm spectral range, this again confirms that the photoelectric conversion of the device originated from the photoexcitation of the Z907 dye. Furthermore, an absorbed photon-to-current conversion efficiency (APCE) value, which means internal quantum efficiency of photoelectric conversion, could be calculated with the formula APCE (%) = IPCE (%) / LHE (%). As shown in Figure 4g, APCE values of the device remained about 60%, which were as high as that of the control SLG/Z907/TiO₂ device (Figure S11d, Supporting Information) and 63% APCE value for Z907-based solid-state dye-sensitized solar cell reported in the literature.^[47] Therefore, the Z907/SLG/TiO₂ heterointerface can be used for effectively separating and collecting photoexcited carriers for photoelectric conversion.

3. Conclusion

This work presented the photovoltaic conversion at an ISET-based heterointerface. With amphiphilic Z907 molecules as a

model dye to fabricate the dye/SLG/TiO₂ ternary interface, the photoexcited electrons in the dye can directly tunnel across SLG with a probability of 99.7% and finally be collected by the TiO₂ layer with an efficiency of 96.23%, which guarantee the high photoelectric conversion at the heterointerface. When monolayer Z907 dyes were uniformly assembled on the surface of SLG/TiO₂ Schottky diode for constructing an ISET-based photovoltaic device, the intrinsic Schottky barrier led to a high photovoltage during photovoltaic conversion. More importantly, the preponderant conformation for Z907 assembly on graphene and the synergetic electron–hole transport under an electrostatic attraction effect cause a faster hole collection at the heterointerface, which enables the large fill factor and the good intense-light performance of the photovoltaic device. Therefore, the ISET-based heterointerfaces have great potential to be applied for building high-efficiency photovoltaic devices with easy fabrication.

Supporting Information

Supporting Information is available from the Wiley Online Library or from the author.

Acknowledgements

C.J., W.M., and J.G. contributed equally to this work. The authors thank Prof. Xiaoyuan Hou from Fudan University for his help on transient photovoltage measurements. This work was supported by

the Ministry of Science and Technology of China (2017YFA0204901 and SQ2017YFJC020081) and the National Natural Science Funds of China (Grant Nos. 21373014, 21727806, and 11222431).

Conflict of Interest

The authors declare no conflict of interest.

Keywords

charge transport, graphene, interface, photovoltaics

Received: May 22, 2017

Revised: August 18, 2017

Published online:

- [1] F. H. L. Koppens, T. Mueller, P. Avouris, A. C. Ferrari, M. S. Vitiello, M. Polini, *Nat. Nanotechnol.* **2014**, *9*, 780.
- [2] H. Yuan, X. Liu, F. Afshinmanesh, W. Li, G. Xu, J. Sun, B. Lian, A. G. Curto, G. Ye, Y. Hikita, Z. Shen, S. C. Zhang, X. Chen, M. Brongersma, H. Y. Hwang, Y. Cui, *Nat. Nanotechnol.* **2015**, *10*, 707.
- [3] C. Jia, H. Li, J. Jiang, J. Wang, H. Chen, D. Cao, J. F. Stoddart, X. Guo, *Adv. Mater.* **2013**, *25*, 6752.
- [4] C. Jia, Q. Wang, N. Xin, J. Zhou, Y. Gong, L. Li, Q. Sun, X. Guo, *Adv. Mater. Technol.* **2016**, *1*, 1600067.
- [5] T. Leydecker, M. Herder, E. Pavlica, G. Bratina, S. Hecht, E. Orgiu, P. Samori, *Nat. Nanotechnol.* **2016**, *11*, 769.
- [6] C. Jia, J. Wang, C. Yao, Y. Cao, Y. Zhong, Z. Liu, X. Guo, *Angew. Chem., Int. Ed.* **2013**, *52*, 8666.
- [7] C. Jia, A. Migliore, N. Xin, S. Huang, J. Wang, Q. Yang, S. Wang, H. Chen, D. Wang, B. Feng, Z. Liu, G. Zhang, D.-H. Qu, H. Tian, M. A. Ratner, H. Q. Xu, A. Nitzan, X. Guo, *Science* **2016**, *352*, 1443.
- [8] C. Clavero, *Nat. Photonics* **2014**, *8*, 95.
- [9] X. Li, C. Jia, B. Ma, W. Wang, Z. Fang, G. Zhang, X. Guo, *Sci. Rep.* **2015**, *5*, 14497.
- [10] C. Poelking, M. Tietze, C. Elschner, S. Olthof, D. Hertel, B. Baumeier, F. Wurthner, K. Meerholz, K. Leo, D. Andrienko, *Nat. Mater.* **2015**, *14*, 434.
- [11] C. Jia, X. Li, N. Xin, Y. Gong, J. Guan, L. Meng, S. Meng, X. Guo, *Adv. Energy Mater.* **2016**, *6*, 1600431.
- [12] S. Chen, C. E. Small, C. M. Amb, J. Subbiah, T.-H. Lai, S.-W. Tsang, J. R. Manders, J. R. Reynolds, F. So, *Adv. Energy Mater.* **2012**, *2*, 1333.
- [13] G. Grancini, M. Maiuri, D. Fazzi, A. Petrozza, H. J. Egelhaaf, D. Brida, G. Cerullo, G. Lanzani, *Nat. Mater.* **2013**, *12*, 29.
- [14] X. Guo, N. Zhou, S. J. Lou, J. Smith, D. B. Tice, J. W. Hennek, R. P. Ortiz, J. T. L. Navarrete, S. Li, J. Strzalka, L. X. Chen, R. P. H. Chang, A. Facchetti, T. J. Marks, *Nat. Photonics* **2013**, *7*, 825.
- [15] F. De Angelis, *Acc. Chem. Res.* **2014**, *47*, 3349.
- [16] M. G. Panthani, J. M. Kurley, R. W. Crisp, T. C. Dietz, T. Ezzyat, J. M. Luther, D. V. Talapin, *Nano Lett.* **2014**, *14*, 670.
- [17] S. S. Wilson, J. P. Bosco, Y. Tolstova, D. O. Scanlon, G. W. Watson, H. A. Atwater, *Energy Environ. Sci.* **2014**, *7*, 3606.
- [18] H. Zhou, Q. Chen, G. Li, S. Luo, T. B. Song, H. S. Duan, Z. Hong, J. You, Y. Liu, Y. Yang, *Science* **2014**, *345*, 542.
- [19] H. Xu, H. Ohkita, Y. Tamai, H. Bentes, S. Ito, *Adv. Mater.* **2015**, *27*, 5868.
- [20] C. Jia, W. Ma, C. Gu, H. Chen, H. Yu, X. Li, F. Zhang, L. Gu, A. Xia, X. Hou, S. Meng, X. Guo, *Nano Lett.* **2016**, *16*, 3600.
- [21] C. Gu, C. Jia, X. Guo, *Mater. Chem. Front.* **2017**, <https://doi.org/10.1039/c7qm00230k>.
- [22] I. Chung, B. Lee, J. He, R. P. Chang, M. G. Kanatzidis, *Nature* **2012**, *485*, 486.
- [23] C. Li, M. T. Cole, W. Lei, K. Qu, K. Ying, Y. Zhang, A. R. Robertson, J. H. Warner, S. Ding, X. Zhang, B. Wang, W. I. Milne, *Adv. Funct. Mater.* **2014**, *24*, 1218.
- [24] G. Kresse, J. Furthmüller, *Phys. Rev. B* **1996**, *54*, 18.
- [25] C. Jia, X. Guo, *Chem. Soc. Rev.* **2013**, *42*, 5642.
- [26] C. Jia, B. Ma, N. Xin, X. Guo, *Acc. Chem. Res.* **2015**, *48*, 2565.
- [27] D. Xiang, X. Wang, C. Jia, T. Lee, X. Guo, *Chem. Rev.* **2016**, *116*, 4318.
- [28] Z. Li, X. Zhang, G. Lu, *J. Phys. Chem. C* **2012**, *116*, 9845.
- [29] Z. Li, X. Zhang, G. Lu, *J. Phys. Chem. B* **2010**, *114*, 17077.
- [30] R. Long, W. Fang, O. V. Prezhdo, *J. Phys. Chem. C* **2017**, *121*, 3797.
- [31] A. V. Akimov, A. J. Neukirch, O. V. Prezhdo, *Chem. Rev.* **2013**, *113*, 4496.
- [32] R. Long, D. Casanova, W. Fang, O. V. Prezhdo, *J. Am. Chem. Soc.* **2017**, *139*, 2619.
- [33] T. Lu, W. Li, F. Bai, R. Jia, J. Chen, H. Zhang, *J. Mater. Chem. A* **2017**, *5*, 15567.
- [34] C. C. Jia, J. L. Jiang, L. Gan, X. F. Guo, *Sci. Rep.* **2012**, *2*, 707.
- [35] N. Petrone, C. R. Dean, I. Meric, A. M. van der Zande, P. Y. Huang, L. Wang, D. Muller, K. L. Shepard, J. Hone, *Nano Lett.* **2012**, *12*, 2751.
- [36] K. Yan, H. Peng, Y. Zhou, H. Li, Z. Liu, *Nano Lett.* **2011**, *11*, 1106.
- [37] A. C. Ferrari, J. C. Meyer, V. Scardaci, C. Casiraghi, M. Lazzeri, F. Mauri, S. Piscanec, D. Jiang, K. S. Novoselov, S. Roth, A. K. Geim, *Phys. Rev. Lett.* **2006**, *97*, 187401.
- [38] Y. Cao, Y. Bai, Q. Yu, Y. Cheng, S. Liu, D. Shi, F. Gao, P. Wang, *J. Phys. Chem. C* **2009**, *113*, 6290.
- [39] B. Bouthinon, R. Clerc, J. Vaillant, J.-M. Verilhac, J. Faure-Vincent, D. Djurado, I. Ionica, G. Man, A. Gras, G. Pananakakis, R. Gwoziecki, A. Kahn, *Adv. Funct. Mater.* **2015**, *25*, 1090.
- [40] S. A. Haque, E. Palomares, B. M. Cho, A. N. M. Green, N. Hirata, D. R. Klug, J. R. Durrant, *J. Am. Chem. Soc.* **2005**, *127*, 3456.
- [41] J. A. Christians, D. T. Leighton, P. V. Kamat, *Energy Environ. Sci.* **2014**, *7*, 1148.
- [42] B. C. O'Regan, K. Bakker, J. Kroeze, H. Smit, P. Sommeling, J. R. Durrant, *J. Phys. Chem. B* **2006**, *110*, 17155.
- [43] X. Chen, B. Wu, *Rev. Sci. Instrum.* **2015**, *86*, 013905.
- [44] R. Long, N. J. English, O. V. Prezhdo, *J. Am. Chem. Soc.* **2012**, *134*, 14238.
- [45] B. Qi, J. Wang, *Phys. Chem. Chem. Phys.* **2013**, *15*, 8972.
- [46] Q. Wang, Y. Shao, Q. Dong, Z. Xiao, Y. Yuan, J. Huang, *Energy Environ. Sci.* **2014**, *7*, 2359.
- [47] M. Wang, S.-J. Moon, D. Zhou, F. Le Formal, N.-L. Cevyey-Ha, R. Humphry-Baker, C. Grätzel, P. Wang, S. M. Zakeeruddin, M. Grätzel, *Adv. Funct. Mater.* **2010**, *20*, 1821.